

# Elucidating the Composition and Structure of Uranium Oxide Powders Produced via NO<sub>2</sub> Voloxidation

Kathryn M. Peruski,\* Tyler L. Spano, Matthew C. Vick, Chase Cobble, Allison T. Greaney, and Joanna McFarlane



Cite This: *ACS Omega* 2024, 9, 10979–10991



Read Online

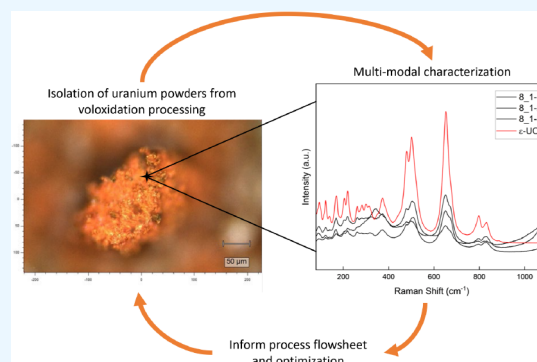
ACCESS |

Metrics & More

Article Recommendations

Supporting Information

**ABSTRACT:** Voloxidation is a potential alternative reprocessing scheme for spent nuclear fuel that uses gas–solid reactions to minimize aqueous wastes and to separate volatile fission products from the desired actinide phase. The process uses NO<sub>2</sub>(g) as an oxidant for uranium dioxide (UO<sub>2</sub>) fuel, ideally producing soluble uranium powders which can then be processed for full recycle. To continue development of the process flowsheet for voloxidation, ongoing examination of the process chemistry and associated process materials is required: discrepancies in the proposed chemical reactions that occur when spent nuclear fuel is exposed to NO<sub>2</sub>(g) atmospheres must be addressed. The objective of this work is to analyze the intermediate solid phases produced during voloxidation to support verification of the proposed NO<sub>2</sub>(g) voloxidation reaction mechanisms. This objective was achieved through using (1) powder X-ray diffraction and Raman spectroscopy to identify bulk uranium phases and (2) scanning electron microscopy to describe the morphology and microstructure of the powders at each reaction stage. The initial oxidation of UO<sub>2</sub> under NO<sub>2</sub>(g) reactions produced  $\epsilon$ -UO<sub>3</sub>. Further exposure to NO<sub>2</sub>(g) did not nitrate the solid to produce uranyl nitrate, as reported in some literature. However, after the powder was hydrated with steam and then further exposed to NO<sub>2</sub>(g), some traces of uranyl nitrate hexahydrate were found. The results of this study suggest that surface hydration of powders plays a vital role in uranyl nitrate formation under voloxidation conditions and raises questions about the kinetics of the oxide-to-nitrate voloxidation conversion process. Future chemical and engineering design decisions for the voloxidation process may benefit from an improved understanding of these chemical mechanisms.



## 1. INTRODUCTION

The continued advancement of commercial spent nuclear fuel reprocessing schemes is essential to the sustainability of the commercial nuclear fuel cycle. The goal of spent fuel reprocessing is the recovery and recycling of uranium (U) from spent fuel, which typically contains 95% UO<sub>2</sub>.<sup>1</sup> Additionally, the recovery of U can be used to separate out the myriad of fission products in the fuel, including fission gases (Xe and Kr), metallic fission products (Mo, Tc, Ru, Rh, and Pd), and oxide fission products (Rb, Cs, Ba, Zr, Sr, and Nb).<sup>1</sup> Currently, spent fuel reprocessing is achieved through aqueous processes such as the PUREX process, which uses solvent extraction to separate U from Pu and other fission products in a tri-*n*-butyl phosphate (TBP) and nitric acid (HNO<sub>3</sub>) two-phase system.<sup>2</sup> Despite the robust nature of the PUREX process and its proven applicability on an industrial scale, current leaders in nuclear fuel separations and reprocessing have identified management of aqueous wastes (primarily HNO<sub>3</sub>) and management of volatile fission products, including <sup>129</sup>I and tritium, as key areas of development needed for simplified and sustainable reprocessing schemes.<sup>3</sup>

Volatile oxidation, or voloxidation, is an alternative reprocessing flowsheet that may reduce aqueous nitrate wastes and can easily separate out problematic volatile fission products. Voloxidation uses gas–solid reactions between an oxidizing gas and spent fuel to produce a soluble uranium oxide phase, which can be used in subsequent aqueous separation processes rather than a traditional aqueous dissolution and separation like PUREX. Early research into process development for a voloxidation flowsheet dates back to the 1970s.<sup>4</sup> Initially, voloxidation was explored with air<sup>4</sup> as the oxidant for the fuel and was found to have the specific advantage of release of <sup>85</sup>Kr, <sup>131</sup>I, and tritium<sup>4</sup> during air voloxidation.<sup>4</sup> More recently, an alternative voloxidation process using NO<sub>2</sub>(g) as the oxidant has been explored. Literature on uranium oxide interactions with NO<sub>2</sub>(g) spans

**Received:** January 2, 2024  
**Revised:** February 2, 2024  
**Accepted:** February 9, 2024  
**Published:** February 23, 2024



over 70 years,<sup>5</sup> but the specific effect of NO<sub>2</sub>(g) as an oxidant for spent fuel has only recently been investigated.<sup>6–9</sup> Initial interest in NO<sub>2</sub>(g) oxidation of spent nuclear fuel was motivated by concerns of NO<sub>2</sub>(g) buildup from gamma radiolysis during dry storage.<sup>10,11</sup> The literature notes that NO<sub>2</sub>(g) was a better oxidant of spent fuel than air, thus prompting subsequent efforts to modify the original air voloxidation process.

Ongoing process engineering research has focused on voloxidation processing of spent nuclear fuel using NO<sub>2</sub>(g) to address the need for alternative fuel reprocessing flowsheets. In the 2010s, a flowsheet for NO<sub>2</sub>(g) voloxidation was developed that focused on concept development,<sup>6,7,12</sup> engineering design of equipment needed for the process,<sup>8</sup> and oxidation mechanisms of uranium oxide solids with NO<sub>2</sub>(g).<sup>9,13</sup> Design and testing of volatile off-gas capture systems were strongly emphasized, as well as analysis of radiiodine.

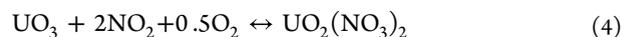
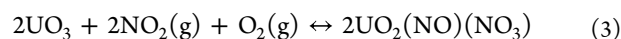
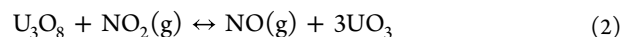
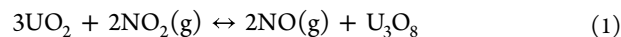
The chemical reactions supporting the NO<sub>2</sub>(g) voloxidation process have been studied most often in a stepwise manner, exploring individual reactions of a specific uranium oxide phase with NO<sub>2</sub>(g) or NO<sub>2</sub>/O<sub>2</sub>(g) mixtures. The reaction of UO<sub>2</sub> with NO<sub>2</sub> was first studied by Katz and Gruen,<sup>5</sup> who noted that the reaction produced something similar to UO<sub>3</sub> or another intermediate oxide. Gimzewski et al.<sup>14</sup> presented a conflicting result, with thermogravimetric data indicating that UO<sub>2</sub> did not react with the mixture of NO<sub>2</sub>/O<sub>2</sub>(g). An important conclusion from the original Katz and Gruen work is that NO<sub>2</sub>(g) may adsorb to the surface of UO<sub>2</sub>,<sup>5</sup> suggesting that this reaction is surface-area dependent. More current research by McEachern et al.<sup>10</sup> supported the hypothesis that NO<sub>2</sub> adsorbs to the surface of UO<sub>2</sub> and acts as a catalyst for surface oxidation. However, McEachern et al. concluded that there are additional intermediate uranium solid phases with the first reaction product of UO<sub>2</sub> oxidation with NO<sub>2</sub> being a U<sub>3</sub>O<sub>7</sub> surface layer followed by U<sub>3</sub>O<sub>8</sub>.<sup>10</sup> These studies indicate that initial surface reactions of UO<sub>2</sub> with NO<sub>2</sub>(g) atmospheres are highly complex, and transformation to higher oxide phases may be kinetically limited by available surface area or buildup of surface oxidation layers.

The direct U<sub>3</sub>O<sub>8</sub> reaction with NO<sub>2</sub> is well documented in the literature, with a consensus that the reaction produces UO<sub>3</sub> under dry conditions.<sup>5,9,10,13,15</sup> If water vapor is also present, then U<sub>3</sub>O<sub>8</sub> has been shown to form soluble uranyl compounds that have been suggested to be uranyl nitrate or uranyl hydroxynitrate.<sup>16</sup> The specific reaction of UO<sub>3</sub> under NO<sub>2</sub>(g) is not well documented. One report uses thermogravimetric data to show that UO<sub>3</sub> reacts with NO<sub>2</sub>(g), and the authors suggest the product may be a uranyl nitrate phase.<sup>14</sup> However, no bulk phase analysis was performed to corroborate this conclusion. An instance of UO<sub>3</sub> reaction with nitric acid indicates the formation of uranyl nitrate,<sup>17</sup> as well.

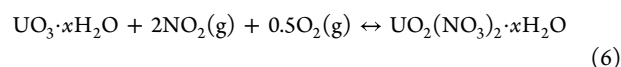
Formation of uranyl nitrate phases from NO<sub>2</sub>(g) oxidation of uranium oxides without adding H<sub>2</sub>O is not well supported by literature evidence. Some reports indicate that dry nitration with NO<sub>2</sub>(g) terminates at the formation of UO<sub>3</sub> and that formation of uranyl nitrate is not reported.<sup>5,10</sup> Alternatively, another study indicates that an NO<sub>2</sub> reaction with U<sub>3</sub>O<sub>8</sub> can produce NO(UO<sub>2</sub>)(NO<sub>3</sub>)<sub>3</sub>,<sup>15</sup> although the kinetics of the reaction are on the order of weeks or months. Additional information suggests that in the presence of water vapor, NO<sub>2</sub>(g) reacts with U<sub>3</sub>O<sub>8</sub> to form soluble uranyl nitrate compounds.<sup>16</sup> These discrepancies in reaction mechanisms

lead to questions about the potential for formation of nitrate compounds and the conditions and time scales required to form uranyl nitrates in NO<sub>2</sub>(g) atmospheres.

Combining the available information on chemical reactions from the literature, the proposed reaction mechanisms of the NO<sub>2</sub>(g) voloxidation process may involve the following sequential oxidation and nitration steps of UO<sub>2</sub>(s):



It is also possible to introduce a hydration step following the oxidation reactions in eq 1 and 2, which could be subsequently nitrated:



Although documentation of voloxidation-type processes has been available for decades, the need remains to elucidate and deconflict the reaction mechanisms and to provide corroborating and direct evidence of reactions using microanalysis of the solid phases involved in the process. Many efforts regarding the voloxidation process have focused on process engineering, flowsheet development, gas-phase analysis, and off-gas capture. Of the studies that probed the chemical reactions of voloxidation, the mechanisms have often been studied for a single step of this process rather than throughout a continuous flowsheet. Furthermore, solid-phase characterization of intermediate and final uranium solid phases is limited in the literature, thus complicating proper identification of reaction steps. Information on solid phases from voloxidation in the literature rely on color of the material<sup>7,18</sup> as a characterization technique and diagnostic method for the solid phase. Recently, Spano et al. identified that for ε-UO<sub>3</sub>, multiple colors can coexist within a single sample, but despite that, crystalline phases and optical vibrational properties are identical.<sup>19</sup> This finding implies that color is not an appropriate characterization technique for uranium oxide materials and underscores that thorough characterization of uranium solids involved in these reactions is imperative. This work aims to provide thorough characterization of uranium solids through a comprehensive suite of solid-phase characterization techniques, including microscopy, diffraction, and spectroscopy, to eliminate any doubt of the solids present throughout this process.

Increased emphasis on the nature of uranium solids through the alternative voloxidation process can provide a better understanding of the chemical phenomena underlying this process and can also provide an opportunity for process optimization and informed flowsheet development. Therefore, the overarching goal of this work is to identify the bulk phases and microstructures of uranium solids during the proposed reaction mechanisms described in eqs 1–6 through sequential characterization of all intermediate and final solid products in the NO<sub>2</sub>(g) voloxidation reactions. Limited solid-phase characterization available in the literature, particularly a lack of multimodal analysis methods, has precluded detailed elucidation of these mechanisms. The application of microscopy and microanalysis to uranium oxide and nitrate

phases is an important addition to the body of literature on uranium solid-state chemistry, given that the materials characterized here are from process applications, which are a helpful comparison to materials generated in a more controlled, laboratory setting. This study aims to provide foundational knowledge on the physical and chemical characteristics of the solid phases involved in this gas–solid process, when so much of the existing literature on the process has focused on the gas phase.

## 2. MATERIALS AND METHODS

Samples for analysis were generated through alternative voloxidation processing, which was performed inside a custom-built gas test loop at Oak Ridge National Laboratory (ORNL). The source material for the voloxidation was depleted  $\text{UO}_2$  fuel pellets spiked with known quantities of simulated (nonradioactive) fission products. These Simfuel pellets were created by mixing commercially prepared nonradioactive oxides and metal powders of select fission products with  $\text{UO}_2$  powder. Fission products included in the fuel pellets are listed in the Supporting Information (Table S1). Mixing was performed by hand. After powder preparation, pellets were pressed using a 10 mm pellet die constructed from D2 tool steel and obtained from Pellet Press Die Sets, Inc. The pellet die, plunger, and anvil were lubricated using a solution of 10 wt % steric acid dissolved in chloroform. Once the chloroform had evaporated, the powder was added to the pellet die and pressed using a 25-ton benchtop manual press obtained from Carver, Inc. Compressive forces of  $\sim 20.0$  kN were used. After preparation,  $\text{UO}_2$  pellets were reacted in the gas testing loop with combinations of  $\text{NO}_2(\text{g})/\text{O}_2(\text{g})$  at elevated temperatures to produce the higher uranium oxide phases according to eqs 1–6. The test conditions listed in Table 1 are based on reported literature transitions for the U–

O system. The proportion of  $\text{NO}_2(\text{g})/\text{O}_2(\text{g})$  was selected from Collins et al.<sup>12</sup> The reaction of  $\text{UO}_2$  in  $\text{NO}_2/\text{O}_2(\text{g})$  has been shown to not proceed at temperatures up to 350 °C,<sup>14</sup> so the initial oxidation step is chosen with temperatures ranging from 350 to 450 °C. Further oxidation of  $\text{U}_3\text{O}_8$  to  $\text{UO}_3$  is reported to occur in temperatures ranging from 250 to 375 °C.<sup>5,18</sup> However, the transition from  $\text{U}_3\text{O}_8$  to  $\text{UO}_3$  is reversible, with the potential to convert back to  $\text{U}_3\text{O}_8$  at temperatures as low as 400 °C.<sup>17</sup> Therefore, the second oxidation step was performed at lower temperatures than in the first step. The hydration was performed in steam, at a temperature of 100 °C. The final nitration step was performed at the same temperature to avoid any reconversion to  $\text{U}_3\text{O}_8$ .

Solid-phase samples were collected from residual powder in the test loop after various steps of the voloxidation process by stopping the test at the desired step and recovering powder. Samples were analyzed using scanning electron microscopy (SEM) coupled with energy-dispersive spectroscopy (EDS), powder X-ray diffraction (pXRD), and Raman spectroscopy. Flowsheets for each test set and its associated analysis are provided in Figure 1.

For SEM-EDS, powders were dry-mounted onto gunshot residue (GSR) tabs, which are double-sided carbon tape affixed to an aluminum pin stub. Samples were analyzed in their as-received condition and were not sputter-coated. SEM-EDS analysis was performed on a Hitachi S4700 field-emission scanning electron microscope equipped with an Oxford Aztec Microanalysis EDS detector at an accelerating voltage of 15 kV with a current of 10  $\mu\text{A}$  and a working distance of 12 mm.

Samples were prepared for pXRD investigations by combining a small quantity of National Institute of Standards and Technology (NIST) 640e Si standard reference material (SRM) with each powder sample provided. Each sample and SRM aliquot was lightly ground to ensure homogeneity and was then transferred to a zero-background silicon substrate. The pXRD data were collected on a PROTO AXRD benchtop powder diffractometer in Bragg–Brentano configuration. Samples were illuminated with a  $\text{Cu K}\alpha$  ( $\lambda = 1.5406$  Å) X-ray source with incident and diffracted beam Soller slits, a 0.5 mm divergence slit, and a diffracted beam nickel  $\beta$ -filter. Diffraction data were collected in the range of 10–75°  $2\theta$ , with a step size of 0.02°  $2\theta$  and a frame length of 2.5 s. Zero shift corrections were performed using the known positions of the (111), (220), (311), and (400) reflections of NIST 640e SRM

**Table 1. Reaction Conditions for Solid Phase Preparation**

step	gases	temperature (°C)
first oxidation	50% $\text{NO}_2$ /50% $\text{O}_2$	350–450
second oxidation	50% $\text{NO}_2$ /50% $\text{O}_2$	250–375
hydration	100% $\text{H}_2\text{O}$	100
nitration	50% $\text{NO}_2$ /50% $\text{O}_2$	<100

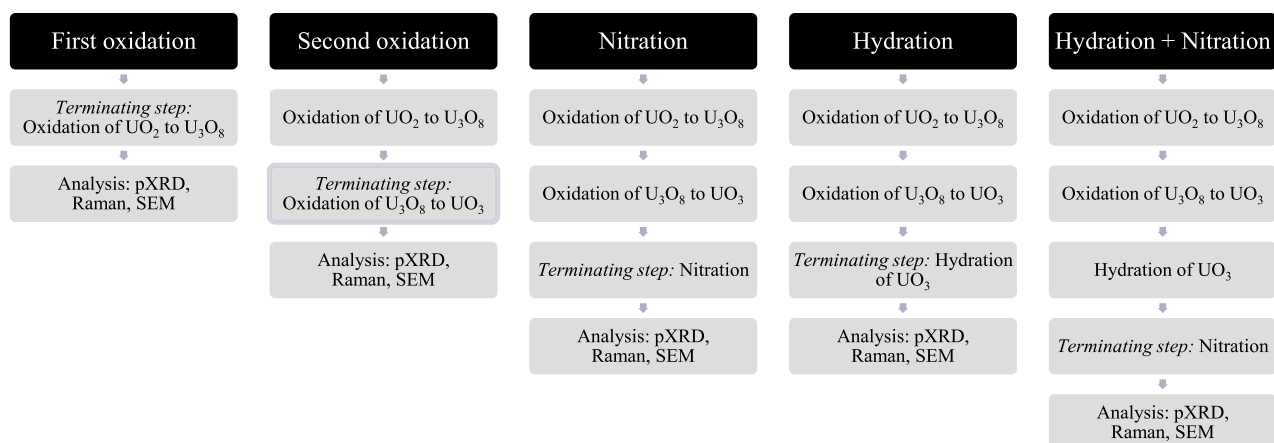


**Figure 1.** Flowsheet of voloxidation testing and solid phase analysis of reaction products.

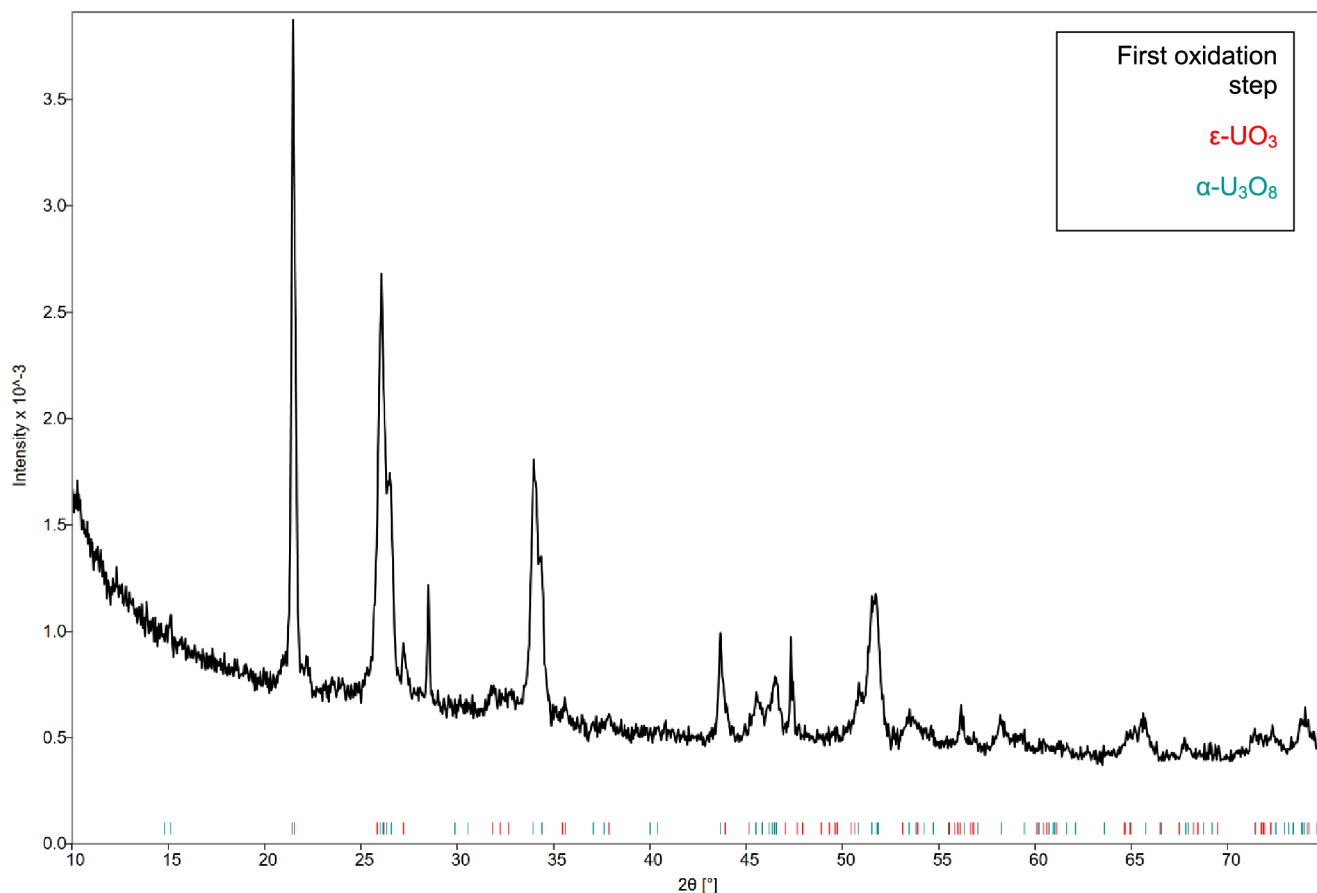


**Figure 2.** pXRD data collected for first oxidation step sample (black trace) compared to  $\epsilon$ - $\text{UO}_3$  and  $\alpha$ - $\text{U}_3\text{O}_8$ .

located at 28.441, 47.300, 56.120, and 69.126°  $2\theta$ , respectively. Data were analyzed using CrystalDiffract and the PDF4+ database.

Raman spectroscopic data were collected using a Renishaw inVia micro-Raman spectrometer on microgram quantities of sample powder that were adhered to GSR tabs. Spectra were collected using a 785 nm excitation wavelength in the range of 35–1,100  $\text{cm}^{-1}$ . Most data collections were 10 accumulations of 1 s of data with a 1% laser power and 20 $\times$  optical magnification. When appropriate, laser power was decreased to 0.5% to prevent laser-induced chemical transformations.

### 3. RESULTS

**3.1. First Oxidation Step.** The initial oxidation of  $\text{UO}_2$  during  $\text{NO}_2$ -based voloxidation, which is expected to produce  $\text{U}_3\text{O}_8$ , produces a uranium powder composed of a mixture of uranium oxide solids with a heterogeneous morphology and microstructure. Macroscopic visualization of the color and texture of the powder in an optical image shows that the powder is fine, mostly black, and cryptocrystalline (Figure S1). Diffraction data collected for the black powder indicate that this sample is a mix of  $\epsilon$ - $\text{UO}_3$ <sup>20</sup> and  $\alpha$ - $\text{U}_3\text{O}_8$ <sup>21</sup> (Figure 2). Further analysis of the powder via Raman spectroscopy corroborates the presence of mixed uranium oxide phases, including  $\epsilon$ - $\text{UO}_3$  and  $\alpha$ - $\text{U}_3\text{O}_8$ . A broad background in the Raman spectra (Figure 3) ranging between  $\sim$ 175 and 500  $\text{cm}^{-1}$  suggests that additional phases, including  $\alpha$ - $\text{U}_3\text{O}_8$  may be present.

Micrographs of the powder after the initial oxidation step show clumped agglomerates with a mixture of rounded and

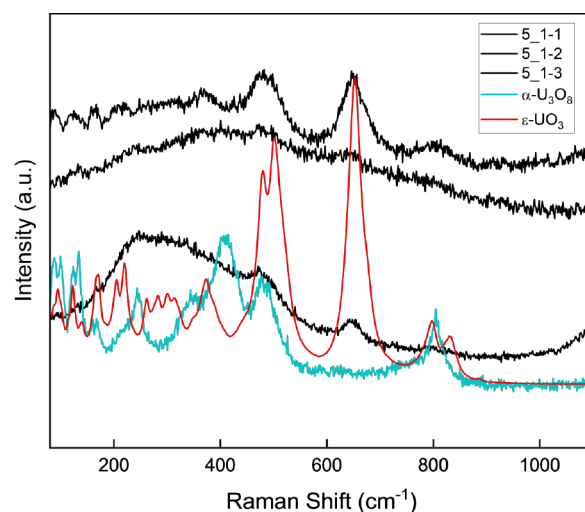


**Figure 3.** Raman spectra collected for first oxidation step sample (sample ID 5\_1-1, 5\_1-2, and 5\_1-3) compared with the spectra of  $\epsilon$ - $\text{UO}_3$ <sup>20</sup> and  $\alpha$ - $\text{U}_3\text{O}_8$ <sup>21</sup>.

platy subparticles (Figure 4). Within the agglomerate, there is evidence of some layering of the platy particles, as well as clumping or irregular aggregation of grains. The size of full agglomerates is very heterogeneous, ranging from single micron to hundreds of microns in diameter. The platy and rounded subparticles are in the size range of hundreds of nanometers.

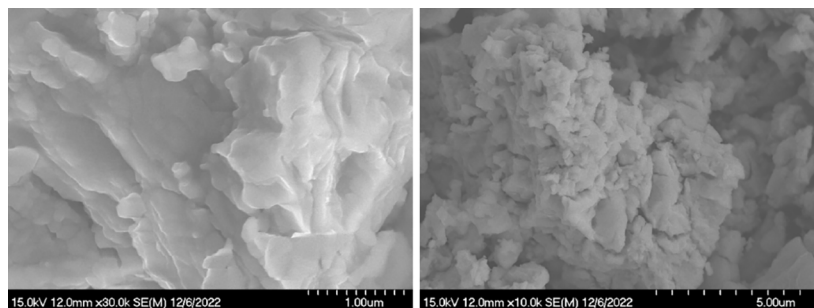


Figure 4. Scanning electron micrographs from the first oxidation step sample.

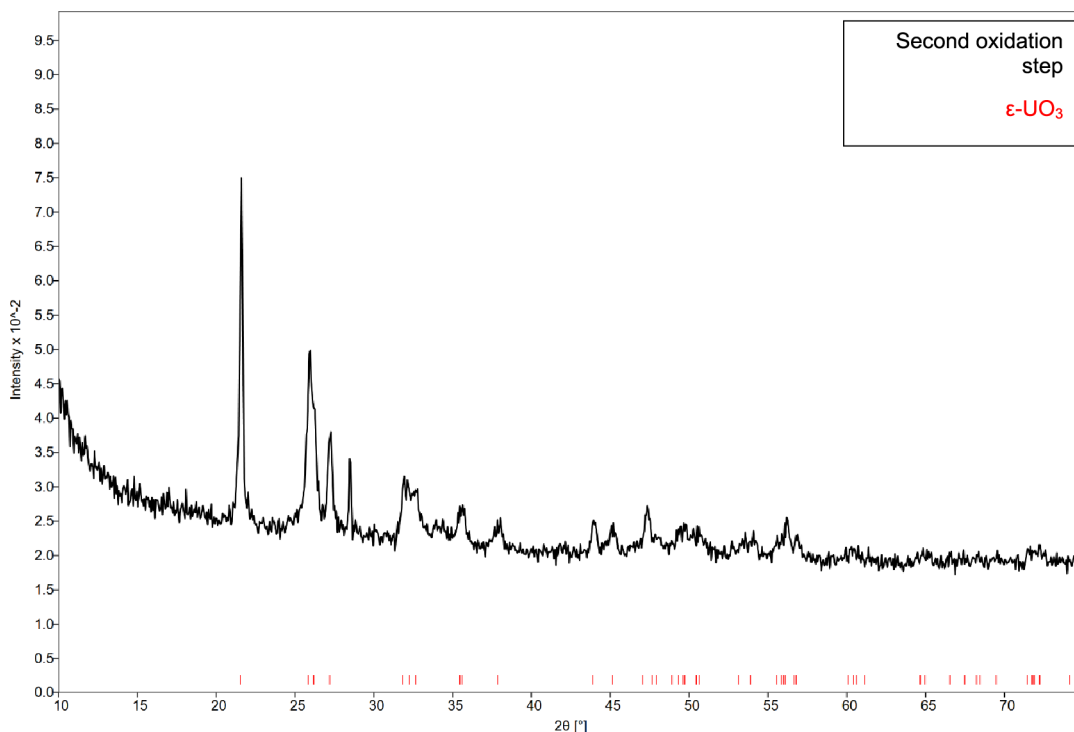


Figure 5. pXRD data collected for second oxidation step (black trace) compared to  $\epsilon$ - $\text{UO}_3$ .

**3.2. Second Oxidation.** The second oxidation step during  $\text{NO}_2$ -based voloxidation, which was expected to produce  $\text{UO}_3$ , showed evidence of  $\text{UO}_3$ , with potential contributions from a minor hydroxide phase. Samples from two separate tests of this step have varying results from bulk phase analysis. The first sample from the second oxidation step contains bright orange cryptocrystalline powder, as well as additional black particles (Figure S2). The appearance of this sample, particularly the mixture of orange and black particles, is consistent with observations from Spano et al. for  $\epsilon$ - $\text{UO}_3$ .<sup>20</sup>

The pXRD data for the sample support the visual interpretation, showing the presence of peaks associated with  $\epsilon$ - $\text{UO}_3$  (Figure 5). There is noise in the diffraction pattern of Figure 5 which, coupled with the broad features present in the Raman spectra (Figure 6), suggest that  $\epsilon$ - $\text{UO}_3$  is poorly crystalline. The average crystallite domain size, determined by Scherrer calculation, is 39.45 nm.

The sample from the second test analyzing the second oxidation step alternative voloxidation has an appearance similar to that of the first sample, with bright orange cryptocrystalline particles; however, it is notably missing the black particles observed in the first sample (Figure S3). pXRD

results indicate that this phase is primarily composed of  $\epsilon$ - $\text{UO}_3$  with minor contributions to the diffractogram from  $\beta$ - $\text{UO}_2\text{OH}_2$  (Figure 7). Observation of Raman spectra further confirms that the major phase of the sample is  $\epsilon$ - $\text{UO}_3$  (Figure 8), and the unidentified vibrational mode at  $\sim 340\text{ cm}^{-1}$  is likely attributable to  $\beta$ - $\text{UO}_2\text{OH}_2$ .

Micrographs of the two samples from the second oxidation step show similarities in microstructure and morphology. Both contain massive agglomerates composed of layered, platy subparticles (Figure 9). The agglomerate size is on the order of microns to tens of microns, whereas the subparticles are hundreds of nanometers. Cracking is evident within the agglomerates as well.

**3.3. Dry Nitration.** Dry nitration of the uranium oxide solid does not produce uranyl nitrate, as suggested in eqs 3 and 4. The resulting powder from dry nitration is bright orange in appearance (Figure S4) and is similar in physical appearance to the powders from the second oxidation step. Like the samples from the second oxidation step, the diffraction data indicate a primary  $\epsilon$ - $\text{UO}_3$  phase with minor contributions to the diffractogram from  $\beta$ - and/or  $\alpha$ - $\text{UO}_2\text{OH}_2$  (Figure 10). The presence of  $\epsilon$ - $\text{UO}_3$  as the primary bulk uranium phase in the

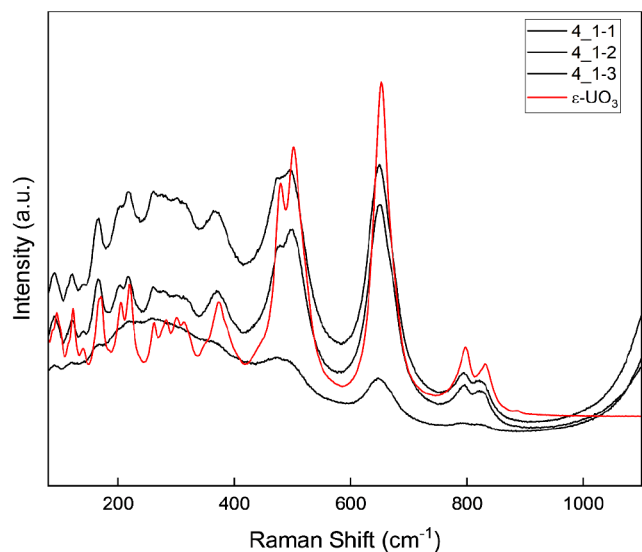


**Figure 6.** Raman spectra collected for second oxidation step sample 1 (sample ID 4\_1). Broadening of vibrational modes is observed and suggests poor crystallinity of the sample.

powder was confirmed further through examination of Raman spectra (Figure 11), which are in good agreement with the published spectra for  $\epsilon$ - $\text{UO}_3$ . An additional low-intensity but sharp vibrational mode was observed at  $\sim 820 \text{ cm}^{-1}$  for one particle from the sample, indicating the presence of a uranyl hydroxide phase.

The morphology of the solids from the attempted nitration step is unique within this series of samples. The clumped

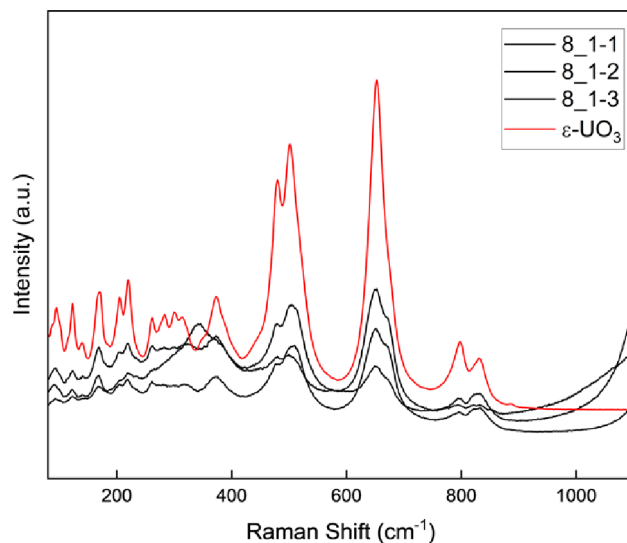


**Figure 8.** Raman spectra collected for second oxidation step sample 2 (black traces) compared with published spectra for  $\epsilon$ - $\text{UO}_3$  (red trace). Sample from the second oxidation step was numbered 8\_1.

agglomerates, which are tens of microns in diameter, are composed of rounded granulates (Figure 12). The granules are clumped such that clear grain boundaries are lacking, and attribution of grain size is not possible. The platy, flaky, or cracked features which were seen in Figures 5 and 11 are not present in this process step.

**3.4. Hydration.** The suggested prehydration step shown in eq 5 following the two oxidation steps yields a heterogeneous

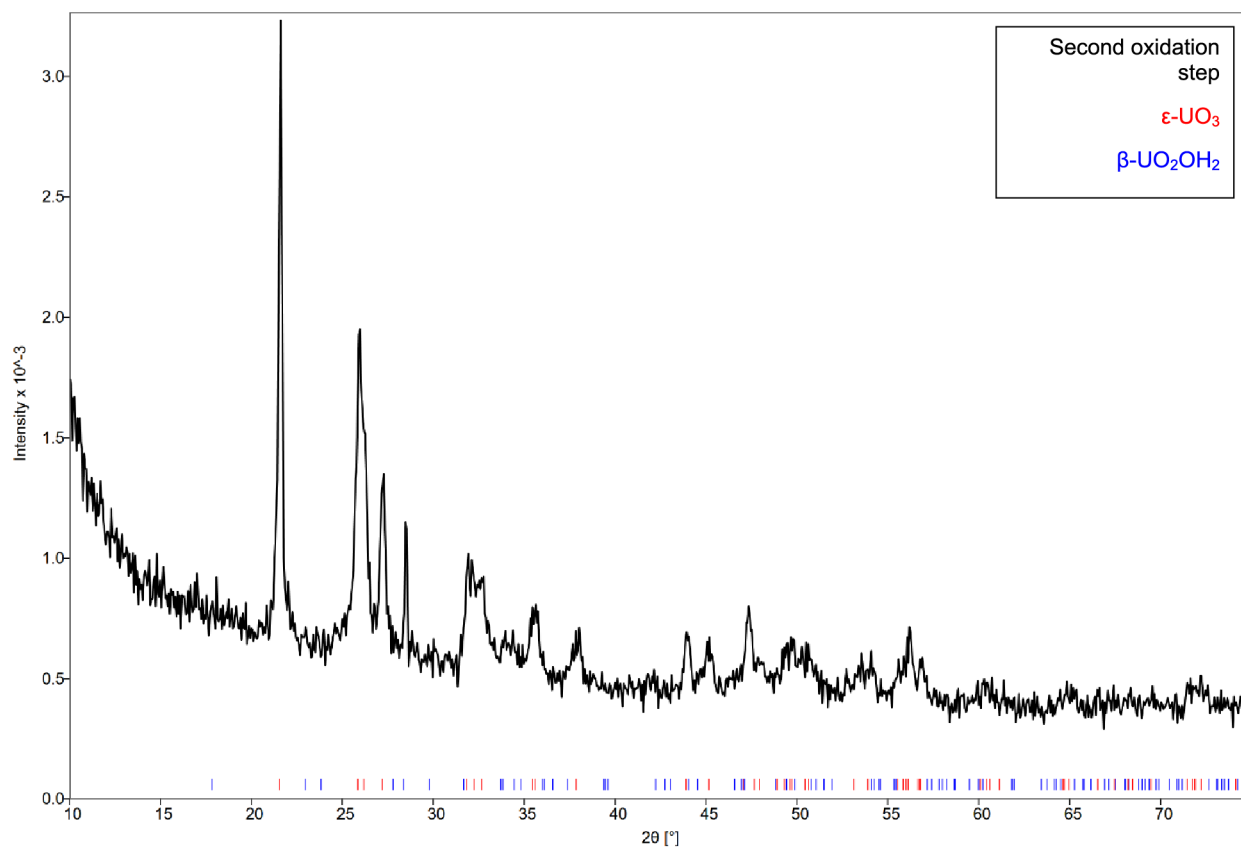


**Figure 7.** pXRD data for the second oxidation step sample 2 (black trace) compared to diffractograms for  $\epsilon$ - $\text{UO}_3$  and  $\beta$ - $\text{UO}_2\text{OH}_2$ .

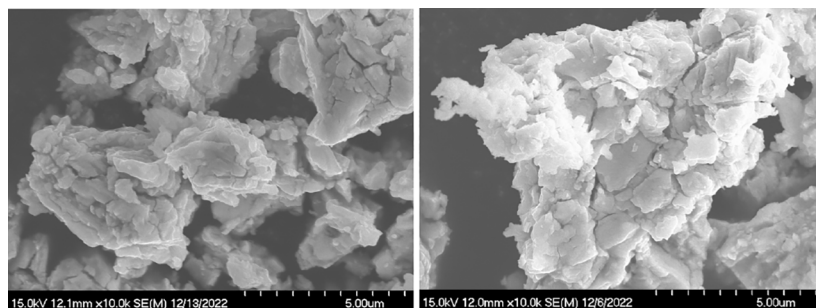


Figure 9. Scanning electron micrographs of first sample (left) and second sample (right) from the second oxidation step.

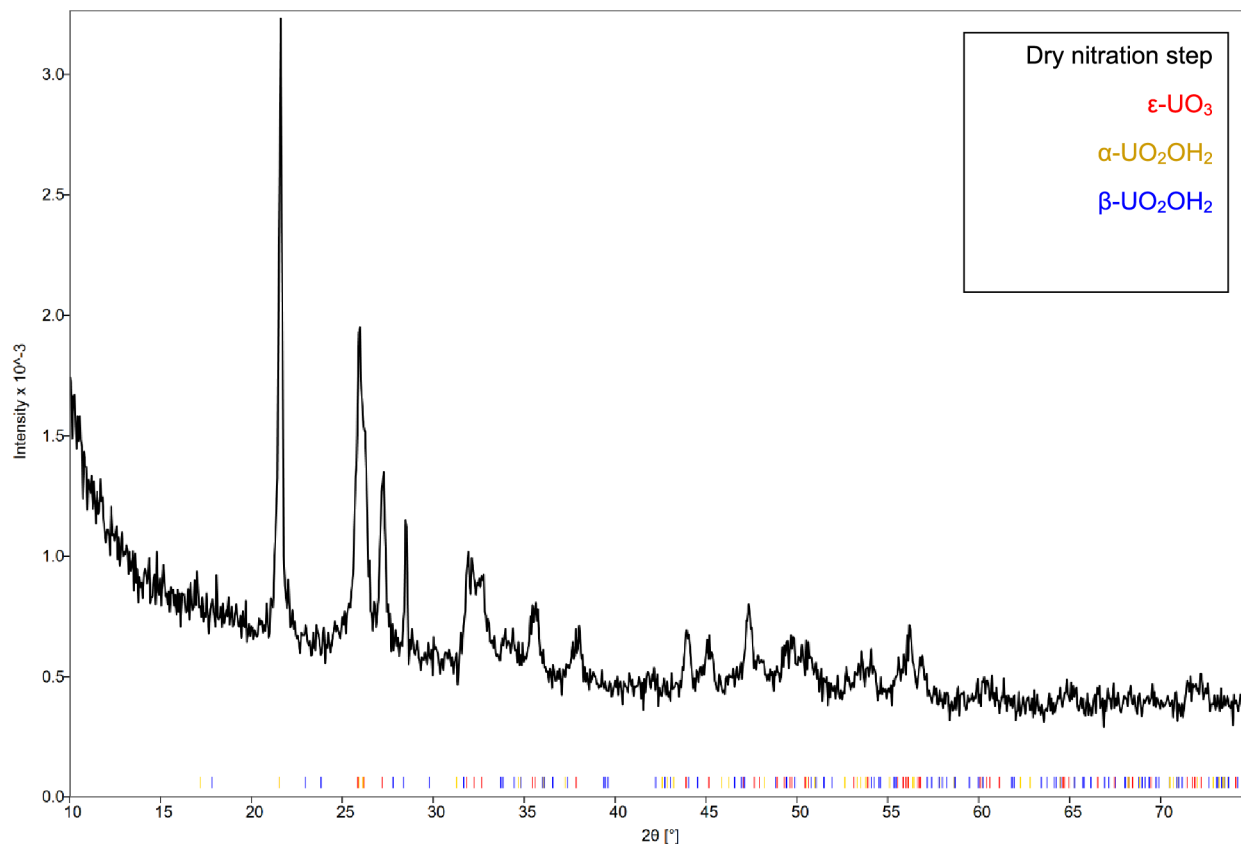


Figure 10. pXRD data for nitration attempt (black trace) compared to diffractograms for  $\epsilon$ - $\text{UO}_3$ ,  $\alpha$ - $\text{UO}_2\text{OH}_2$ , and  $\beta$ - $\text{UO}_2\text{OH}_2$ .

mixture of hydrated uranyl phases with distinct, reticulated plate morphology. The exposure to steam produces a bulk phase which is bright yellow in color, with additional smaller particles that are a mix of yellow and black (Figure S5).

Numerous uranyl hydroxide phases, including  $\text{UO}_3 \cdot 0.8\text{H}_2\text{O}$ ,  $(\text{UO}_2)_8(\text{OH})_{12} \cdot 12\text{H}_2\text{O}$  (synthetic schoepite,<sup>23</sup> and  $\alpha$ - $\text{UO}_2\text{OH}_2$ ,<sup>24</sup> are observed in pXRD data (Figure 13). Similarly, Raman spectra collected for powders after hydration are consistent with observations of a uranyl hydroxide hydrate phase presented by Kirkegaard et al.<sup>25,26</sup> (Figure 14), and additional broad vibrational modes suggest that  $\alpha$ - $\text{U}_3\text{O}_8$  may be present.

The morphology and microstructure of the hydrated powder sample are unlike the previously observed structures from the oxidation steps. The clumped agglomerates, which are on the order of tens of microns in diameter, contain two distinct subparticle types: reticulated plates and reticulated subrounded grains (Figure 15), which are consistent with the appearance of

uranyl hydroxide phases. These two microstructures can both be seen within the same larger aggregate. Most previously observed samples have displayed layered, platy substructures with some granular features.

**3.5. Hydration + Nitration.** As observed in the hydration step sample, the powder sample after hydration described in eq 5 and the subsequent attempted nitration presented in eq 6 are multiphase and heterogeneous. The similarity of the hydration and hydration + nitration samples is consistent with the samples in which the hydration step is the origin material for the nitration. The sample from hydration + nitration contains a bright yellow powder, as well as some bright orange particles (Figure S6).

Phase identification of the powders after hydration + nitration is complex because of contributions from multiple uranyl phases. pXRD data (Figure 16) indicate that this sample is primarily composed of  $\text{UO}_3 \cdot 1-0.8\text{H}_2\text{O}$ , with minor contributions from  $\alpha$ - $\text{U}_3\text{O}_8$ . Interestingly, reflections attrib-

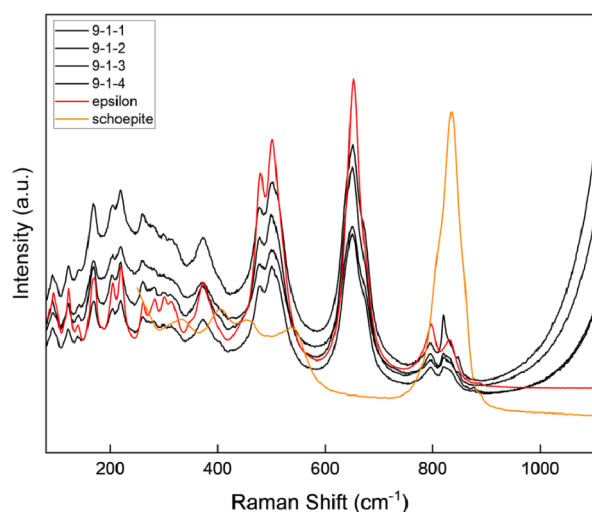


**Figure 11.** Raman spectra collected for nitration attempt (sample IDs 9-1, 1-4) compared with published spectra for  $\epsilon$ - $\text{UO}_3$  and the uranyl hydroxide mineral phase schoepite obtained from the RRUFF database.<sup>22</sup>

able to uranyl nitrate trihydrate are visible in the diffractogram for this phase. The multiple phases observed from pXRD are also visible in Raman spectra collected for the same sample, although significant fluorescence is observed. The region where symmetric stretching of the  $\text{UO}_2^{2+}$  ion<sup>27,28</sup> appears ( $\sim 750$ – $900 \text{ cm}^{-1}$ ) shows multiple bands (Figure 17), indicating that multiple uranium coordination environments<sup>29</sup> are present in the phases within the hydrated + nitrated sample. Because of the observed complexity of this sample, 16 individual Raman spectra were collected. Two of the spectra are consistent with mostly pure uranyl nitrate trihydrate, with minor  $\epsilon$ - $\text{UO}_3$  contributions (6\_2-1-15 and 6\_2-1-16, Figure 17). Several other spectra show evidence of uranyl nitrate contributions (e.g., 6\_2-1-1 and 6\_2-1-6) in combination with uranyl hydroxide and perhaps  $\epsilon$ - $\text{UO}_3$  vibrational modes (Figure 17).

Micrographs of the powder after both hydration and nitration are very similar to those from the hydration step. Primarily, the sample consists of clumped agglomerates, again with two distinct subparticle types (Figure 18). Agglomerates are approximately tens to hundreds of microns in size. The reticulated plates, which are one submorphology of these agglomerates, are multiple microns in length and tens of nanometers thick. The granular portions of the agglomerate are hundreds of nanometers in diameter.

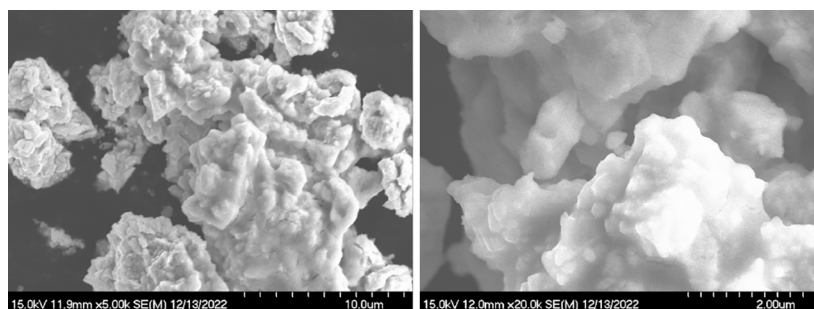


**Figure 12.** Scanning electron micrographs of the dry nitration sample.

#### 4. DISCUSSION

The presumed mechanisms of alternative voloxidation processing have been assessed using stepwise solid-phase characterization of uranium powders from a voloxidation test loop. It is expected that  $\text{UO}_2$  would undergo two oxidation steps upon exposure to  $\text{NO}_2(\text{g})$ , followed by nitration, as shown in eq 1–4. In sequential order, the expected solid phases throughout this process are  $\text{UO}_2(\text{s}) \rightarrow \text{U}_3\text{O}_8(\text{s}) \rightarrow \text{UO}_3(\text{s}) \rightarrow \text{UO}_2(\text{NO}_3)_2$ . Slight alteration of this pathway could occur in the case of hydration of the sample, which would produce  $\text{UO}_3 \cdot x\text{H}_2\text{O}$  and  $\text{UO}_2(\text{NO}_3)_2 \cdot x\text{H}_2\text{O}$  as the final uranium phases. The physical and chemical data collected during this set of experiments suggest that the reaction pathway may not proceed as previously reported in the literature. A summary and comparison of collected physical and chemical data is presented in Table 2. In addition to tracking the physical chemical properties of uranium oxides throughout this process, the fate of fission products was also tracked. However, due to the low weight percent of each fission product in the pellets, compared to the bulk U phases, fission products were not detected conclusively throughout the process and do not appear to alter the spectroscopic or structural features observed in this work.

The initial oxidation of  $\text{UO}_2$  during  $\text{NO}_2$ -based voloxidation produces a uranium powder composed of a mixture of uranium oxide solids with heterogeneous morphology and microstructure. While it is reported that the initial oxidation should form  $\text{U}_3\text{O}_8$ , in this work,  $\epsilon$ - $\text{UO}_3$  was observed to be the predominant U phase, with minor  $\text{U}_3\text{O}_8$ . This suggests that the kinetics of the first oxidation may be more rapid than expected. However, the first two oxidation steps produce primarily  $\text{UO}_3$ , which is in agreement with the expected reaction mechanisms and the literature evidence of  $\text{UO}_2$  oxidation in  $\text{NO}_2(\text{g})$ .<sup>5,10</sup> The formation of this specific polymorph when  $\text{U}_3\text{O}_8$  is exposed to  $\text{NO}_2(\text{g})$  has been previously reported,<sup>9,18</sup> but the production of  $\epsilon$ - $\text{UO}_3$ , specifically the  $\epsilon$  polymorph of  $\text{UO}_3$ , is notable, suggesting that a  $\text{U}_3\text{O}_8$  precursor exists during oxidation, because all reported production methods for  $\epsilon$ - $\text{UO}_3$  require  $\text{U}_3\text{O}_8$  and a pseudomorphic decomposition reaction from  $\text{U}_3\text{O}_8$  to  $\epsilon$ - $\text{UO}_3$ , which has been suggested in previous works.<sup>20,30,31</sup> Furthermore, the presence of this phase, with only minor  $\text{U}_3\text{O}_8$  contributions, supports the posed hypothesis of rapid kinetics during the initial oxidation step. The microstructural features seen during the first two oxidation steps, particularly cracking in the surface of the uranium oxide phases, suggest that the gases present in the reaction may be acting within grain boundaries or other pre-existing surface anomalies in the ceramic. This may help facilitate the rapid changes to the bulk phase suggested in the pXRD data.

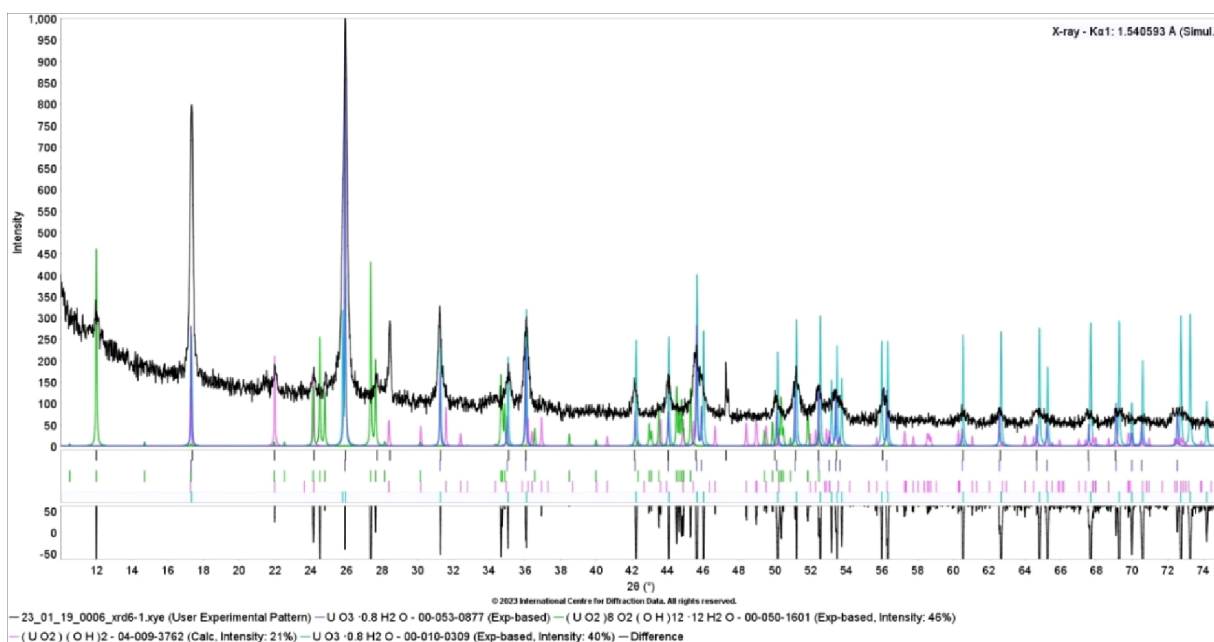


**Figure 13.** pXRD data collected for powder after hydration (black trace), suggesting the presence of multiple uranyl hydroxide phases.

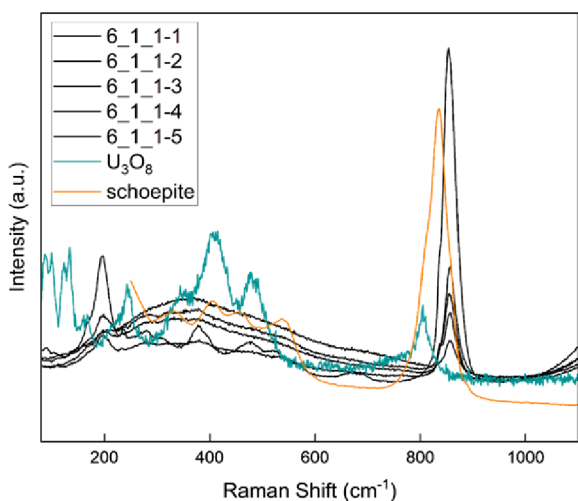


**Figure 14.** Raman spectra collected for powder after hydration (black trace) compared with published spectra for  $\alpha$ - $\text{U}_3\text{O}_8$ <sup>21</sup> (teal) and schoepite— $(\text{UO}_2)_8\text{O}_2(\text{OH})_{12}\cdot 12\text{H}_2\text{O}$ <sup>22</sup> (orange). Samples from hydration step were numbered 6\_1.

Additionally, the observed heterogeneity in the microstructure and bulk phase could be due to the reaction occurring preferentially in cracks or grain boundaries of the material and not acting on the bulk surfaces.

The data collected in this effort suggest that alternative voloxidation does not result in formation of uranyl nitrate phases in dry conditions, but it may form minor nitrate phases following steam hydration and subsequent nitration. The data imply that, after forming higher uranium oxides, the uranium solid does not proceed to the nitrosyl nitrate or nitrate phases in the dry system, which is consistent with some findings in literature.<sup>5,10</sup> It is possible that the reaction kinetics for the formation of uranyl nitrate from  $\text{UO}_3$  are sufficiently slow, as described by Kobets and Klavst,<sup>15</sup> and that the reaction cannot be observed on the time scales of this experiment. The morphological changes to the surface of the powders after dry

nitration (Figure 12) as compared to the initial oxidation steps (Figures 4 and 9) suggest that continued surface alteration and reactions are occurring, despite the lack of bulk phase change. Furthermore, the significant change in microstructure of the uranium solid at this stage may even be due to a surface coating on the solid. However, the reaction may be limited by the available surface area of the initial powder, a factor which was not evaluated in this study but warrants further investigation.

Overall, the steam hydration step appears to have the greatest effect on the physical and chemical properties of the uranium powders tested in this analysis. The hydration step results in a complex mixture of hydrated phases, colorimetric change, and significant morphological change. These altered properties are retained during subsequent nitration. A critical finding from the hydration process is that after the combination of hydration and nitration, the uranium powders show some evidence of a uranyl nitrate trihydrate phase. This suggests that the hydration step may be a critical intermediary for forming nitrate phases. Hydration of  $\text{UO}_3$  evidently alters the morphology and microstructure of the material, particularly the available surfaces of the solid. The complete restructuring of the U solid from a layered, platy agglomerate with cracking to reticulated plate structures suggests there may be additional reactions, such as dissolution and reprecipitation of the material, to cause such changes. Surface hydration and changes to surface area and microstructure of the material may create the pathway for further oxidation of the available U on the surface of the powders.

The proposed reaction mechanisms described in the Introduction are not fully supported by the data collected here. Although the initial oxidation steps agree with literature, the ability of dry nitration of uranium oxides to form uranyl nitrate appears inhibited, whereas the nitration of a hydrated phase appears possible. Further study of the reaction mechanisms in alternative voloxidation processes is warranted to elucidate the role of hydration on uranium phase changes; similarly, additional investigations of the reaction kinetics are

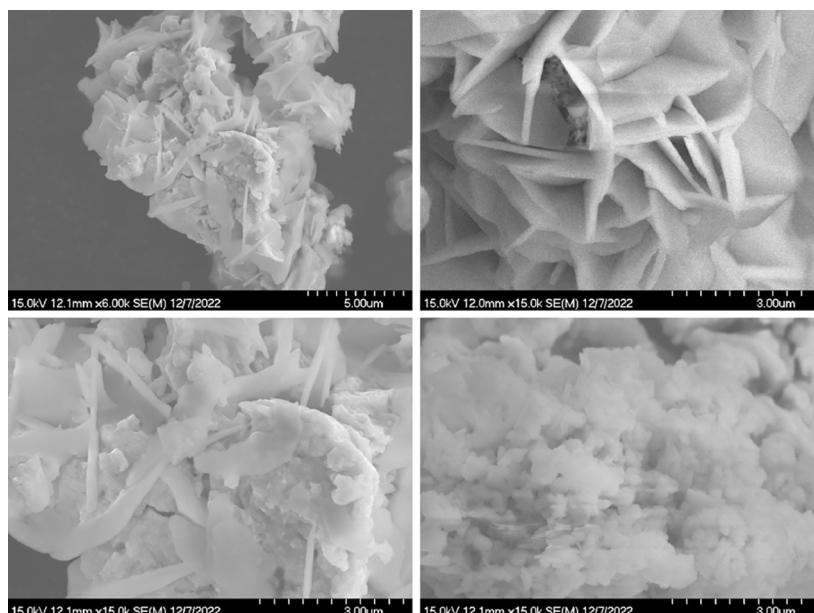


Figure 15. Scanning electron micrographs of powder after hydration.

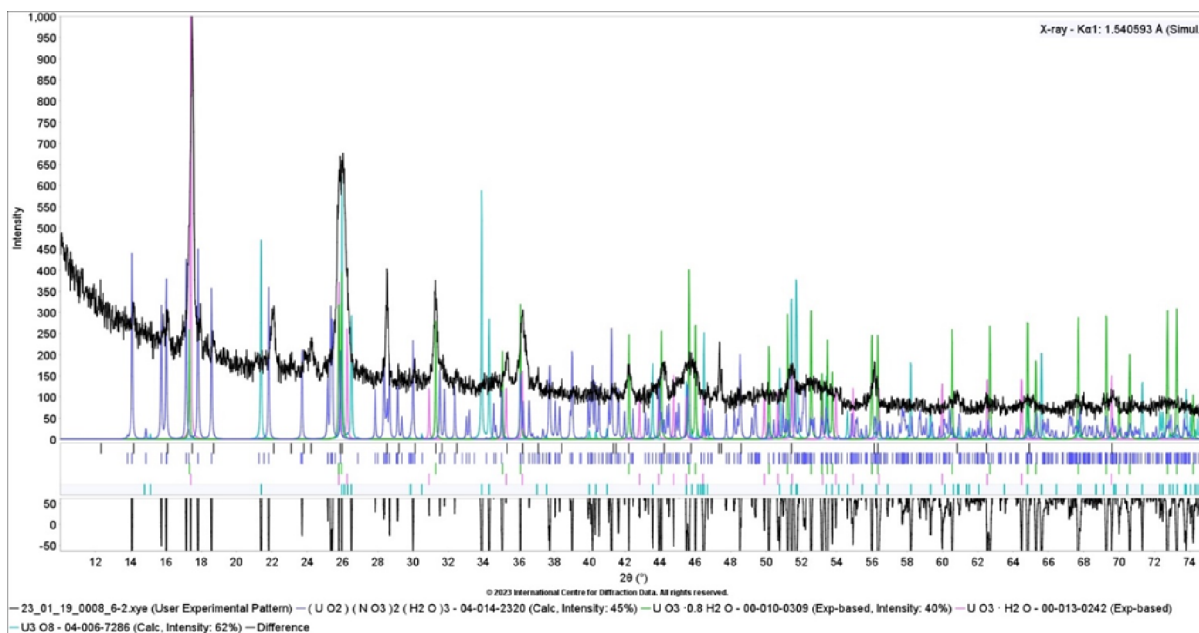


Figure 16. pXRD collected for powder sample after wet nitration (black trace). Reference diffractogram for uranyl nitrate trihydrate is in blue.

warranted to determine if reactions are possible on reasonable process time scales.

## 5. CONCLUSIONS

Solid-phase characterization of uranium powders from the alternative voloxidation process was performed to verify proposed reaction mechanisms and to identify intermediate and final solid products. SEM was utilized to identify morphological and microstructural features of powders and to allow for comparison between process steps. pXRD and Raman spectroscopy were used to identify uranium crystal phases in powders. Overall, solid-phase characterization of voloxidation reaction products indicated that the uranium solid-state chemical system is more complex than initially assumed. Initial oxidation reactions in the presence of  $\text{NO}_2(\text{g})$

produced  $\epsilon\text{-UO}_3$ , but a dry nitration attempt did not produce uranyl nitrate. However, when  $\epsilon\text{-UO}_3$  was first hydrated by steam and then subsequently nitrated, some traces of uranyl nitrate trihydrate were identified. Additionally, hydration caused significant changes to the observed microstructure of the U phase. These findings suggest that surface hydration of uranium oxide may hold the key to favorability of reactions and nitrate phase formation. These data are the first complete microanalysis of uranium solid phases at each step of the alternative voloxidation process, providing valuable insight into uranium oxide phases as well as augmenting process knowledge for flowsheet development. The augmentation of available chemical and physical analysis of these intermediate uranium phases can be used to inform future engineering design decisions and sets a precedence for thorough analysis of

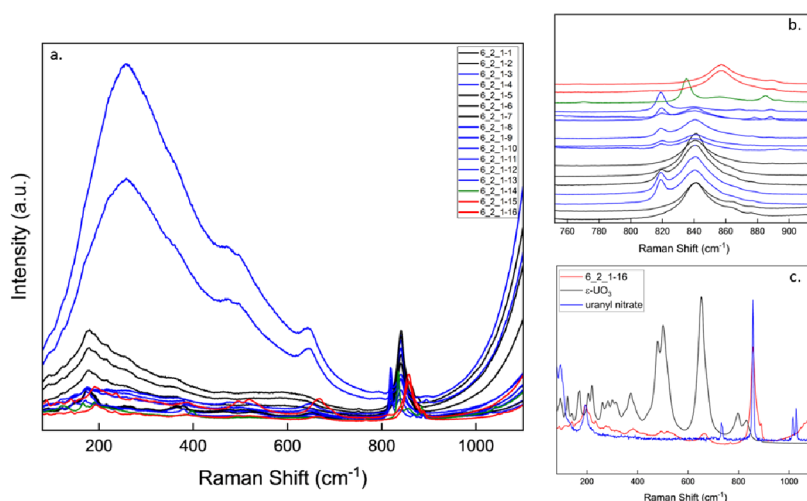


**Figure 17.** Raman spectra collected for powder sample after wet nitration. a. Significant sample fluorescence is observed. b. Multiple U coordination environments are evidenced by numerous bands in the uranyl region ( $\gamma$  offset for clarity). c. Some spectra are consistent with uranyl nitrate.

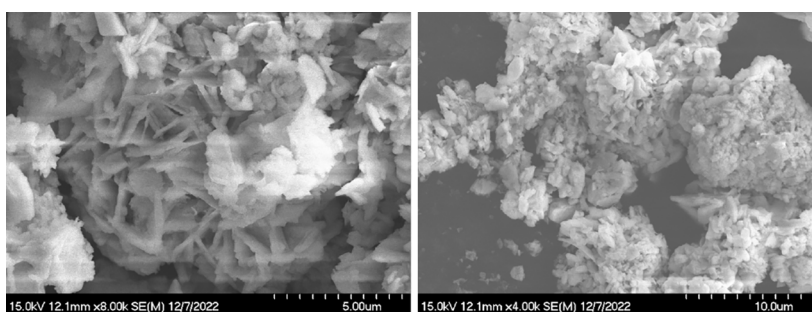


**Figure 18.** Scanning electron micrographs of powder sample after wet nitration.

**Table 2. Summary of Physical and Chemical Characteristics of Uranium Solids from Voloxidation Tests**

step	major phase	minor phase (s)	color	morphology and microstructure
first oxidation	$\epsilon$ - $\text{UO}_3$	$\alpha$ - $\text{U}_3\text{O}_8$	black	agglomerate with platy and granular subparticles
second oxidation	$\epsilon$ - $\text{UO}_3$		orange + black	agglomerate with platy subparticles
	$\epsilon$ - $\text{UO}_3$	$\beta$ - $\text{UO}_2\text{OH}_2$	orange	agglomerate with platy subparticles
nitration	$\epsilon$ - $\text{UO}_3$	$\alpha$ - $\text{UO}_2\text{OH}_2$	orange	agglomerate with rounded granules
		$\beta$ - $\text{UO}_2\text{OH}_2$		
hydration		$\text{UO}_3 \cdot 0.8\text{H}_2\text{O}$	yellow + black	clumped agglomerate with reticulated plates and reticulated subrounded grains
		$(\text{UO}_2)_8(\text{OH})_{12} \cdot 12\text{H}_2\text{O}$		
hydration + nitration	$\text{UO}_3 \cdot \text{H}_2\text{O}$	$\alpha$ - $\text{UO}_2\text{OH}_2$	yellow + orange	clumped agglomerate with reticulated plates and reticulated subrounded grains
		$\text{UO}_3 \cdot 0.8\text{H}_2\text{O}$		
		$(\text{UO}_2)_8(\text{OH})_{12} \cdot 12\text{H}_2\text{O}$		
		$\alpha$ - $\text{UO}_2\text{OH}_2$		
		$\alpha$ - $\text{U}_3\text{O}_8$		
		$\text{UO}_2(\text{NO}_3)_2 \cdot 3\text{H}_2\text{O}$		

both gas and solid phases throughout this process. This work indicates that the alternative voloxidation process chemistry requires further fundamental chemical study, particularly related to the solid phases generated throughout these reactions. Additional studies require quantification of the effects of surface area, particle size, and initial pellet microstructure for better applicability of the chemistry to multiple fuel types in real systems.

## ■ ASSOCIATED CONTENT

### Supporting Information

The Supporting Information is available free of charge at <https://pubs.acs.org/doi/10.1021/acsomega.4c00029>.

Table S1: Elemental composition of Simfuel pellets processed in voloxidation tests, Figure S1: Optical image collected from first oxidation step sample, Figure S2: Optical images collected from second oxidation step, Figure S3: Optical image of second oxidation step sample 2, Figure S4: Optical image of powder after dry

nitration attempt, Figure S5: Optical images collected for hydration step, and Figure S6: Optical images from powder sample from wet nitration (PDF)

## AUTHOR INFORMATION

### Corresponding Author

Kathryn M. Peruski — Oak Ridge National Laboratory, Oak Ridge, Tennessee 37830, USA; Email: [peruskikm@ornl.gov](mailto:peruskikm@ornl.gov)

### Authors

Tyler L. Spano — Oak Ridge National Laboratory, Oak Ridge, Tennessee 37830, USA; [orcid.org/0000-0001-6572-9722](https://orcid.org/0000-0001-6572-9722)

Matthew C. Vick — Oak Ridge National Laboratory, Oak Ridge, Tennessee 37830, USA

Chase Cobble — Oak Ridge National Laboratory, Oak Ridge, Tennessee 37830, USA

Allison T. Greaney — Oak Ridge National Laboratory, Oak Ridge, Tennessee 37830, USA

Joanna McFarlane — Oak Ridge National Laboratory, Oak Ridge, Tennessee 37830, USA

Complete contact information is available at:

<https://pubs.acs.org/10.1021/acsomega.4c00029>

### Author Contributions

The manuscript was written through contributions of all authors. All authors have given approval to the final version of the manuscript.

### Funding

This work was supported by the US Department of Energy, Office of Nuclear Fuel Cycle and Supply Chain, Material Recovery and Waste Form Development Campaign (NE-43) under contract number DE-AC05-00OR22725 at the Oak Ridge National Laboratory.

### Notes

The authors declare no competing financial interest.

## ACKNOWLEDGMENTS

The authors wish to thank R. D. Hunt and G. Del Cul for helpful discussions of this work and its implications.

## REFERENCES

- (1) Bruno, J.; Ewing, R. C. Spent nuclear fuel. *Elements* **2006**, *2* (6), 343–349.
- (2) McKibben, J. M. Chemistry of the purex process. *Radiochim. Acta* **1984**, *36* (1–2), 3–16.
- (3) Moyer, B. A.; Lumetta, G. J.; Bruffey, S. H.; Finkeldei, S.; Marsden, K. C.; Simpson, M. F.; Jensen, M. P.; Zalupski, P. R.; Clark, A. E.; Yang, P.; Gregory, P. H. *Innovative Separations Research and Development Needs for Advanced Fuel Cycles*; Oak Ridge National Lab (ORNL): Oak Ridge, TN (United States), 2022.
- (4) Goode, J. *Voloxidation: Removal of volatile fission products from spent LMFBR fuels*; Oak Ridge National Lab: Oak Ridge, TN, 1973.
- (5) Katz, J.; Gruen, D. Higher oxides of the actinide elements. The preparation of Np<sub>3</sub>O<sub>8</sub>. *J. Am. Chem. Soc.* **1949**, *71* (6), 2106–2112.
- (6) Del Cul, G. D.; Collins, E. D.; Spencer, B. B.; Jubin, R. T. Conceptual Design of a Simplified Head-End Process for the Recycling of Used Nuclear Fuel. *Trans. Am. Nucl. Soc.* **2012**, *106*, 183–184.
- (7) DelCul, G. D.; Spencer, B. B.; Hunt, R. D.; Jubin, R. T.; Collins, E. D. Advanced head-end for the treatment of used LWR fuel. *Actinide And Fission Product Partitioning And Transmutation*. **2010**, 265.
- (8) Johnson, J. A.; DelCul, G. D. *Reaction System Design for NO<sub>2</sub> Oxidation of Used Nuclear Fuel for the FY17 Hot Test*; Oak Ridge National Laboratory: Oak Ridge, TN, 2016.
- (9) Johnson, J. A.; Rawn, C. J.; Spencer, B. B.; Meisner, R. A.; Del Cul, G. D. Oxidation kinetics for conversion of U<sub>3</sub>O<sub>8</sub> to ε-UO<sub>3</sub> with NO<sub>2</sub>. *J. Nucl. Mater.* **2017**, *490*, 211–215.
- (10) McEachern, R. J.; Sunder, S.; Taylor, P.; Doern, D. C.; Miller, N. H.; Wood, D. D. The influence of nitrogen dioxide on the oxidation of UO<sub>2</sub> in air at temperatures below 275° C. *J. Nucl. Mater.* **1998**, *255* (2–3), 234–242.
- (11) Campbell, T. K.; Gilbert, E. R.; White, G. D.; Piepel, G. F.; Wrona, B. J. Oxidation Behavior of Nonirradiated UO<sub>2</sub>. *Nucl. Technol.* **1989**, *85* (2), 160–171.
- (12) Collins, E. D.; Delcul, G. D.; Hunt, R. D.; Johnson, J. A.; Spencer, B. B. Advanced dry head-end reprocessing of light water reactor spent nuclear fuel. US 8,747,790 B2, 2013;
- (13) Johnson, J. A. Studies of reaction processes for voloxidation methods. Ph.D., University of Tennessee, 2013.
- (14) Gimzewski, E.; Hawkins, S. H. Reactions of metal oxides with NO<sub>2</sub> (g) + O<sub>2</sub> (g). *Thermochim. Acta* **1986**, *99*, 379–382.
- (15) Kobets, L.; Klavut, G. Behavior of U 3 O 8 in dissociating gaseous dinitrogen tetroxide. *Soviet Radiochemistry* **1987**, *28* (6), 657–660.
- (16) Kulyukhin, S.; Nevolin, Y. M. Kinetics of gas-phase conversion of U 3 O 8 into water-soluble compounds in nitrating atmosphere at 25–30°C. *Radiochemistry* **2016**, *58*, 144–148.
- (17) Katz, J. J.; Rabinowitch, E. *The Chemistry of Uranium, Part 1, The Element, Its Binary and Related Compounds*; McGraw-Hill Book Company, Inc., 1951.
- (18) Hoekstra, H. R.; Siegel, S. The uranium-oxygen system: U<sub>3</sub>O<sub>8</sub>-UO<sub>3</sub>. *J. Inorg. Nucl. Chem.* **1961**, *18*, 154–165.
- (19) Spano, T. L.; Hunt, R.; Kapsimalis, R. J.; Niedziela, J. L.; Shields, A. E.; Miskowicz, A. Optical vibrational spectra and proposed crystal structure of ε-UO<sub>3</sub>. *J. Nucl. Mater.* **2022**, *559*, 153386.
- (20) Spano, T. L.; Hunt, R.; Kapsimalis, R. J.; Niedziela, J.; Shields, A. E.; Miskowicz, A. Optical Vibrational Spectra and Proposed Crystal Structure of ε-UO<sub>3</sub>. *J. Nucl. Mater.* **2022**, *559*, 153386.
- (21) Miskowicz, A.; Niedziela, J. L.; Spano, T. L.; Ambrogio, M. W.; Finkeldei, S.; Hunt, R.; Shields, A. E. Additional complexity in the Raman spectra of U<sub>3</sub>O<sub>8</sub>. *J. Nucl. Mater.* **2019**, *527*, 151790.
- (22) Lafuente, B.; Downs, R. T.; Yang, H.; Stone, N. The power of databases: the RRUFF project. In *Highlights in Mineralogical Crystallography*; De Gruyter, 2016; pp. 130.
- (23) Plášil, J. The crystal structure of uranyl-oxide mineral schoepite, [(UO<sub>2</sub>)<sub>4</sub>O(OH)<sub>6</sub>](H<sub>2</sub>O)<sub>6</sub>, revisited. *J. Geosci.* **2018**, *63* (1), 65–73.
- (24) Frost, R. L.; Cejka, J.; Weier, M. L. Raman spectroscopic study of the uranyl oxyhydroxide hydrates: becquerelite, billietite, curite, schoepite and vandendriesscheite. *J. Raman Spectrosc.* **2007**, *38* (4), 460–466.
- (25) Kirkegaard, M. C.; Ambrogio, M. W.; Miskowicz, A.; Shields, A. E.; Niedziela, J.; Spano, T. L.; Anderson, B. B. Characterizing the degradation of [(UO<sub>2</sub>F<sub>2</sub>)(H<sub>2</sub>O)]<sub>7</sub>·4H<sub>2</sub>O under humid conditions. *J. Nucl. Mater.* **2020**, *529*, 151889.
- (26) Kirkegaard, M. C.; Spano, T. L.; Ambrogio, M. W.; Niedziela, J. L.; Miskowicz, A.; Shields, A. E.; Anderson, B. B. Formation of a uranyl hydroxide hydrate via hydration of [(UO<sub>2</sub>F<sub>2</sub>)(H<sub>2</sub>O)]<sub>7</sub>·4H<sub>2</sub>O. *Dalton Trans.* **2019**, *48* (36), 13685–13698.
- (27) Bartlett, J. R.; Cooney, R. P. On the determination of uranium-oxygen bond lengths in dioxouranium (VI) compounds by Raman spectroscopy. *J. Mol. Struct.* **1989**, *193*, 295–300.
- (28) Lu, G.; Haes, A. J.; Forbes, T. Z. Detection and identification of solids, surfaces, and solutions of uranium using vibrational spectroscopy. *Coord. Chem. Rev.* **2018**, *374*, 314–344.
- (29) Burns, P. C.; Ewing, R. C.; Hawthorne, F. C. The crystal chemistry of hexavalent uranium: polyhedron geometries, bond-valence parameters, and polymerization of polyhedra. *Can. Mineral.* **1997**, *35*, 1551–1570.
- (30) Kovba, L.; Vidavskii, L. M.; Lavut, E. G. Study of ε-UO 3. *J. Struct. Chem.* **1964**, *4*, 573–574.

(31) Tsvigunov, A.; Kuznetsov, L. On the low-temperature oxydation of  $\text{UO}_2$ ,  $\text{U}_3\text{O}_8$  and  $\text{U}_3\text{O}_{(8-x)}$  phase by nitrogen dioxide. *Radiokhimiya* **1976**, *18* (3), 411–413.